Modeling of harmonic propagation of fast DC EV charging station in a Low Voltage network

S. Cassano, F. Silvestro
Department of Electrical, Electronic, Telecommunication
Engineering and Naval Architecture
University of Genoa, Genova, Italy
federico.silvestro@unige.it

E. De Jaeger, C. Leroi
Institute of Mechanics, Materials and Civil Engineering
Université Catholique de Louvain
Louvain, Belgium
caroline.leroi@uclouvain.be

Abstract—**During the last decades, the electric scenario has considerably changed, moving towards a more sustainable society. With the power grid development, the inclusion of new energy sources and consumption devices becoming more and more complex, a broader understanding of the interaction between these elements and the electrical system is required. Electrical equipment and the use of electricity are developing towards more energy-efficient and high-technology products and this has an impact on the power quality as well. This paper will focus on harmonic disturbances in the frequency range between 2 and 150 kHz, which are often referred to by the term supraharmonics, aiming to develop a modeling procedure of an EV battery charger emitting supraharmonics in order to quantify them. The model is thought to be as generic as possible, in order to recreate the phenomenon and to be able to study it into details. Simulations have been performed with MATLAB/Simulink® environment and more specifically the Simscape PowerSystems toolbox.**

Index Terms—**EV charging station, supraharmonics, Storage modeling, harmonic emission.**

I. Introduction

Recent changes in the electric grid have brought to light new issues in the fields of study of electrical engineering. Among other, harmonic disturbances in the frequency range between 2 and 150 kHz, often referred to by the term "supraharmonics" or "high frequency (HF) harmonics", has lately gained more interest.

The reason is that on one hand, the amount of devices containing active power electronics is increasing, which could result in an increase in voltage and current distortion in this frequency range. On the other hand, the increasing use of the Power Line Carrier (PLC) involves equipments such as "smart metering", so that the intentional and the so-called "unintentional" emissions coexist in this frequency band.

The main problem was related to a lack of harmonization in the standards covering this range, which are supposed to regulate the emission of the disturbances and the immunity of sensitive devices. Compatibility levels have been defined very recently and probably emission and immunity limits will follow soon based on these levels.

Another particularity of this range consists in the peculiar way the disturbances propagate: HF-harmonic currents mainly flow between the different electronic equipments instead of upstream in the grid [1]. The consequence is that the properties of individual devices have a much bigger influence on HF harmonics than on Low Frequency (LF) harmonics. Therefore, one cannot study a device independently but has to consider the whole installation in order to predict the HF harmonic disturbance levels [2]. Moreover, with the increased levels of HF harmonics, resonances could become an issue.

In this context, different bodies and institutions are working to this common purpose: the European committee for electrotechnical standardization (CENELEC) has already published three reports concerning electromagnetic interferences in this frequency range [3][4][5].

There are many articles in the literature concerning the disturbances produced by different types of equipment [6][7]. This work aim to give a contribution to this wide problematic by investigating on EV charging station, which was chosen due to the likely wide spread of this type of equipment on the distribution network in the near future.

Chapter II shows the actual design of the building blocks of the complete model. Chapter III focuses on the used steps to simplify the model. Chapter IV suggests a model of the Low-Voltage (LV) Grid valid in the frequency range under concern. Chapter V studies the interaction between several devices in terms of primary and secondary emissions.

Modelling and simulation are used in order to investigate the propagation of disturbances and the interaction between other devices through the grid.

II. Complete Model

The fast charging obviously solves the problem of charging time, however a fast charging station with even few fast charging slots, may ask a charging capacity in megawatt range. The high power required has disturbing consequences on the power system, as it can cause an excessive voltage deviation, overload and increase in peak load. Many conditions must thus be met in order to allow the fast charging station to function properly, as shown in TABLE I.

The current trend is to obtain a topology that allows the bi-directionality of the power flow and the integration of Battery Energy Storage (BES) and Renewable Energy Sources (RES) in order to mitigate the aforementioned problems coming from the high charging power required from fast charging station

978-1-5386-4722-6/19/$31.00 ©2019 IEEE

TABLE I
COMPARISON OF DIFFERENT CHARGING STATION TOPOLOGIES [9].

Topology Type	Bidirectional	Grid Support	RES Integration	BES Integration	Power Density	Reliability	
						Component Count (PE)	Control Complexity
Bidirectional AC/DC/DC	Yes	All*	Yes	Yes	Medium	Low	Low
Unidirectional AC/DC/DC	No	APF	No	Yes	Medium	Low	Low
Multiport with common AC-bus	Yes	V2G	No	No	Low	High	Low
Transformerless with DC-link	Yes	All*	Yes	Yes	High	High	High
Transformerless without DC-link	Yes	All*	Yes	Yes	High	High	High
Matrix front-end converter	Yes	PFC, S2G	No	Yes	Medium	High	High

*- bidirectional power transfer, S2G, V2G, APF.

[8]. In this paper, the focus is on EV battery charger that can be implemented in a LV grid.

The bidirectional AC/DC/DC Battery Charger Type seems to be the most suitable since it provides all of the desired features (see Fig.1). The DC/DC conversion chain is expected to enable the link of more devices on a common DC bus.

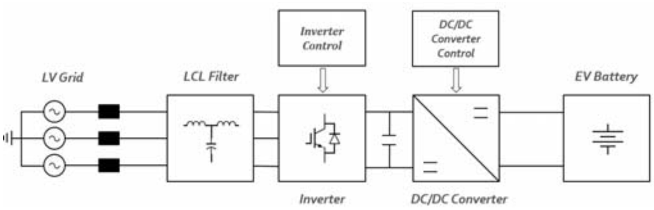

Fig. 1. Complete charging station model

A. Converters and Control

The conversion chain consists of a three-phase PWM controlled Inverter and a bi-directional DC/DC converter that charges an EV battery.

1) Inverter: The inverter is controlled in order to ensure two main functions:

- The DC-link capacitor voltage is maintained constant in order to assure the active power exchange from the battery to the grid;
- The reactive power is controlled in order to have zero absorption at grid side.

Therefore, active and reactive power control can be achieved using Park's transformation. In particular, the direct and the quadrature components of the voltage are used separately to control respectively the DC-link voltage and the reactive power exchange. A PLL is generally needed to generate those components.

2) Bi-directional DC/DC Converter: Constant current strategy is the converter control technique that is used in the battery charger in which the measured current ($i.e.$ the current that flows from/to the battery) is compared with the reference, which is set at the desired value of 125 A. The duty cycle only varies between 0 and 1; therefore, a translator is required to convert the error between the actual current and the reference to something in that range, which is the PI, that needs to be tuned. Once the duty cycle is obtained, this value is compared with a saw tooth signal to obtain pulses ($i.e.$ zeros and ones) that go to the IGBT.

In both cases, the switching frequency was chosen to a value of 5 kHz, which is a typical value for this kind of applications.

B. Passive Elements

1) DC-link Capacitance: The DC-link capacitance has to support the DC current and so, the stability of the bus depends directly on the DC capacitance size. According to [10] the DC capacitance is determined by the capacitor energy rate of change during transient and the rated active power.

2) LCL Filter: In the research about harmonic reduction of grid-interfaced distributed power sources, especially when applied above several kilo-watts, passive LCL filters are turning to state of the art. This trend can also be linked to the problem that creating an L filter would result in great expense, because of its larger size. Designing LCL filter parameters is complex and demands to take in consideration many constraints, such as current ripple, filter size, switching ripple attenuation and reactive power absorbed by the filter capacitor, etc. Method proposed in [11] was used to identify the filter parameters.

3) EV Battery: The Battery block, provided in the SimPowerSystems Library [12], implements a generic dynamic model parameterized to represent most popular types of rechargeable batteries: the parameters of the equivalent circuit can be modified to represent a particular battery type. In this work, a Lithium-Ion battery with a capacity of 35 kWh was chosen since it represents a good average value between the existing EV batteries.

Some of the most important parameters used in the design of the charging station are summarized in TABLE II. The whole charging station is made of a maximum of 4 chargers under condition of full charging power and its rated capacity S_{rated} includes an overload factor for cover overloading in transients.

TABLE II
CHARGING STATION PARAMETERS

Parameters	Values
S_{rated}	200 kVA
$V_{grid,ph-ph}$	400 V
EV charging current	125 A
P_{EV}	45 kW
Battery Capacity	35 kWh
f_{sw}	5000 Hz
$C_{DC-link}$	18 mF
$L_{inv-side}$	0.48 mH
C_f	165μF
$L_{grid-side}$	0.69 mH
R_d	1.31Ω

C. Harmonics

Simulations in Simulink environment, especially the use of the FFT tool, allow to find current and voltage spectra. Phase-to-line voltage harmonics at the output of the inverter will be dealt with. Its harmonic spectrum consists in the fundamental component and harmonics around multiples of the switching frequency, as will further be shown in next section.

III. Simplified Models

Simplification is provided in order to increase the computation speed of the simulation. Besides, a certain accuracy level is maintained. The process is divided into two steps.

A. First Step: Influence of the Downstream Circuit

The first step in simplification consists in examining the weight of the downstream circuit on the grid-side harmonics. The downstream circuit includes the EV battery and the DC-DC bidirectional converter. Simulation were performed in order to investigate the effect of the different switching frequencies of the DC/DC converter on the amplitude of the harmonics on the grid side. The order of magnitude of the DC-link capacitance was also modified. Five different switching frequencies of the DC/DC converter were fixed while three values of the DC-link capacitance were changed in order to see different filtering actions.

The impact of the switching frequency of the switch of the DC/DC converter on the harmonics on the grid side is low ($i.e.$ order of magnitudes), allowing us to replace the downstream circuit with an ideal DC current source.

B. Second Step: Double Fourier Series Analysis

A starting point in the research for an explicit formulation of the output harmonics of naturally sampled PWM is the application of the double Fourier integral form to the problem, as first presented by Black [13]. It can be demonstrated that the Switching Function $S(x, y)$ of the switch of the inverter can be represented by a double Fourier series. Therefore, it is possible to write the phase-to-line voltages by using the switching function:

$$\begin{aligned} v_A \;=\; & \frac{1}{2} r V_d sin(\omega_s t + \phi) + \sum_{m=1}^{\infty} \sum_{n=-\infty}^{\infty} \\ & \left((mod(n,2) - 1) sin\left(\frac{m\pi}{2}\right) \frac{4V_d}{3\pi m} J_n(mQ) \times \right. \\ & \left(1 + cos\left(\frac{n\pi}{3} - 1\right)\right) cos((mp+n)\omega_s t + n\phi) \\ & + mod(n,2) cos\left(\frac{m\pi}{2}\right) \frac{4V_d}{3\pi m} J_n(mQ) \times \\ & \left. \left(1 + cos\left(\frac{n\pi}{3}\right)\right) sin((mp+n)\omega_s t + n\phi) \right) \quad (1) \end{aligned}$$

Where r is the modulation index, V_d the DC-link Voltage, ω_s the fundamental frequency at the output of the inverter, p the ratio between the carrier frequency and this fundamental frequency and ϕ the phase of the modulating wave.

Simulations have been performed using both the complete model and the analytical representation of the inverter in order to compute the amplitude and phase of voltage harmonics. The second step in simplification is related to the comparison between the voltage harmonics in both cases. TABLE III shows the results for phase-to-line harmonics, evaluated at the output of the inverter on the grid side. The error, in percentage, between the harmonics coming from the complete model and the analytical calculations was deemed acceptable: in the worst case, it consists in a value of 2.44% for the harmonic at 14900 Hz.

TABLE III
Phase-to-line voltage harmonics comparison

Frequency (Hz)	Complete Model	Calculations	$\epsilon_{\%}$
4900 Hz	94.27 V	94.61 V	0.36%
5100 Hz	93.30 V	94.61 V	1.38%
9950 Hz	103.93 V	103.58 V	0.33%
10050 Hz	104.94 V	103.58 V	1.31%
14800 Hz	46.53 V	46.79 V	0.55%
14900 Hz	53.04 V	54.37 V	2.44%
15100 Hz	55.63 V	54.37 V	2.31%
15200 Hz	45.87 V	46.79 V	1.96%

The second step in simplification was achieved. The inverter was replaced by a voltage source controlled by a MATLAB code, in order to simulate its harmonics, by using the "MATLAB function" block on Simulink. The simplified model is shown in Fig.2.

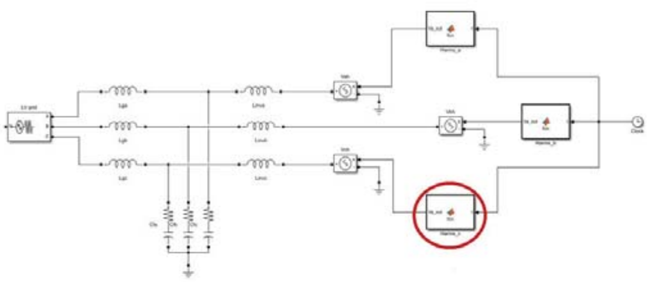

Fig. 2. Simplified Model

IV. LV Distribution Grid HF Model

Modelling the LV distribution grid valid at high frequency is of great importance because it allows us to study the phenomena in a more realistic way. Moreover, most of the time models found in literature are available in low frequencies. The main differences between a LF and HF model is that in HF capacitors are not neglected, and resistances are higher because of the skin effect.

In this paper we focused on the modelling of the LV feeder, since only the interaction between devices will be taken into account. The three-phase PI section line model provided by SimPowerSystems has been adopted [14]. For sake of simplicity the model has been assumed without neutral wiring.

Concerning the values of the parameters, they come out from the comparison between several references ($i.e.$ Laborelec [15], Nexans [16], CIGRE [17] and Electric Power Research Institute [18]). The three-phase PI section line block requires the translation of those parameters in the positive and zero sequences parameters. These are summarized in TABLE IV.

Because of the skin effect, multiple resistances depending on the frequency should be used to study the propagation of different harmonics. But, in lumped elements models (such as those used in SimPowerSystems), a single (constant) value has

TABLE IV
PARAMETERS OF THE THREE-PHASE PI SECTION LINE

R_d	$0.210\ \Omega/km$
R_0	$0.840\ \Omega/km$
L_d	$3.858 \cdot 10^{-4} H/km$
L_0	$1.543 \cdot 10^{-3} H/km$
C_d	$3.354 \cdot 10^{-7} F/km$
C_0	$2.445 \cdot 10^{-7} F/km$

to be fixed. Consequently, a value of the DC resistance R_{DC} was chosen in order to adapt it case by case to the frequency of the harmonic under consideration, according to the skin effect:

$$R = \frac{1}{\sigma 2\pi r\delta} = \frac{r}{2\delta}R_{DC} = \frac{1}{2r}\sqrt{\frac{\mu}{\pi\sigma}}\sqrt{f} \qquad if \;\; r \ll \delta \tag{2}$$

Where δ represent the skin depth

$$\delta = \sqrt{\frac{\rho}{\pi\mu f}}.$$

With r the radius of the conductor (Aluminum), ρ the resistivity of the Aluminum at $25°$ C, μ the permeability of the Aluminum and f the frequency.

V. PROPAGATION OF HF DISTURBANCES

In the study of the propagation of HF disturbances, it is important to distinguish the primary from the secondary emissions:

- $Primary\ emission$: emission coming from the device depending on its "output" impedance. This impedance includes the grid impedance, the filter of the device but also impedance of other connected devices (their EMI filter).
- $Secondary\ emission$: emission generated elsewhere (by other devices, by the grid, etc.) and that propagates into the device due to its low impedance at its terminal.

The basic model of the emission of harmonics by a device is the ideal current/voltage source at the harmonic frequency of interest. The charging station is, here, modeled by a voltage source and the LCL filter at grid side. The grid is initially modeled as a resistance. The complexity of the model will then be increased. As stated before, the grid resistance will be varied case by case depending on the considered harmonic, due to skin effect. Furthermore, we assume that the grid voltage is a pure 50 Hz source (without higher harmonic content), so that it has a zero grid current/voltage source for harmonics above 50 Hz.

A. Effect of the Number of Devices Connected at the same point

The model of two devices connected to the grid is shown in Fig.3. Each equipment is modeled by a voltage source V_h, whose signal is determined by the MATLAB code (see section III B) and an LCL filter. The LCL filter is an important block that has to be considered because it is directly connected to the grid and will play an important role in the interaction among devices.

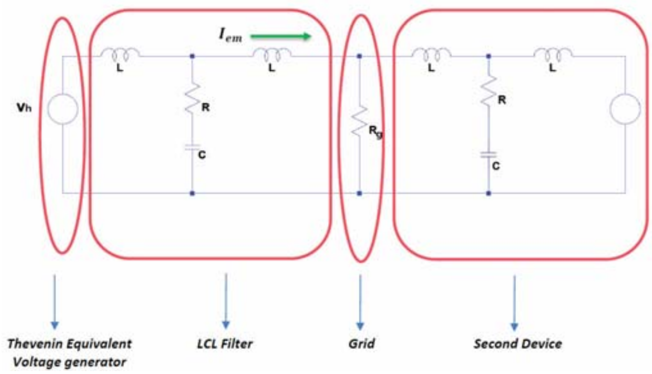

Fig. 3. Simplified model for the study of the interaction of two devices connected to the grid

The emission of a device I_{em} ($i.e.$ the current at the interface between the device and the grid) is the sum of primary and secondary emissions. The maximum number of devices connected to the grid is four, in order not to exceed the limitations in power. We consider all the devices as identical and we take into account the harmonics at 5100 Hz and at 15100 Hz. The experience starts with two devices connected at the same point in the grid; the length of the grid is then increased up to 1 km. Finally, the number of devices increases as well and the simulation is repeated.

1) R Model: Fig.4 and Fig.5 illustrate the influence of the length of the line on the magnitude of the primary and secondary emissions of a maximum of 4 devices. The devices are connected at the same point on the grid in the case of the simplest approximation, which consists in a R-modeled grid. As stated before, the resistance of the grid R_g changes accordingly to the frequency into account due to the skin effect.

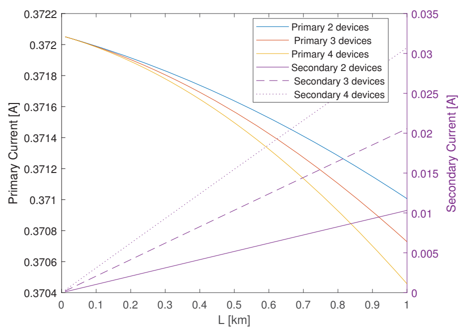

Fig. 4. Effect of the number of connected devices. R Model: primary and secondary emissions of harmonics $n°102$. $V_h = 94.61\angle -4.56°V, R_g = 0.6153\Omega$

2) RL Model: The first step in increasing the complexity of the model is shown in Fig.6 and Fig.7, where the inductance, found in section IV, is inserted in series with the grid resistance.

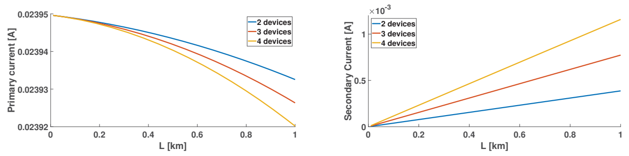

Fig. 5. Effect of the number of connected devices. R Model: primary (left) and secondary (right) emissions of harmonics $n°302$. $V_h = 54.37\angle - 4.56°V, R_g = 1.0587\Omega$

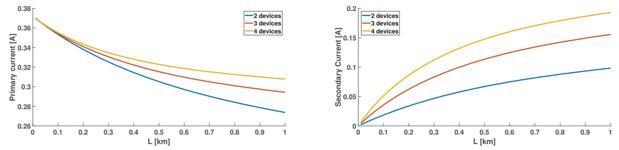

Fig. 6. Effect of the number of connected devices. RL Model: primary (left) and secondary (right) emissions of harmonics $n°102$. $V_h = 94.61\angle - 4.56°V, R_g = 0.6153\Omega$

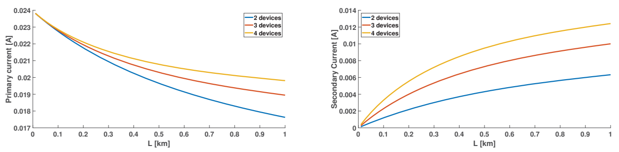

Fig. 7. Effect of the number of connected devices. RL Model: primary (left) and secondary (right) emissions of harmonics $n°302$. $V_h = 54.37\angle - 4.56°V, R_g = 1.0587\Omega$

3) RLC Model: The final step in increasing the complexity of the model is shown in Fig.8 and Fig.9 and consists in inserting the capacitance (split in two), found in section IV.

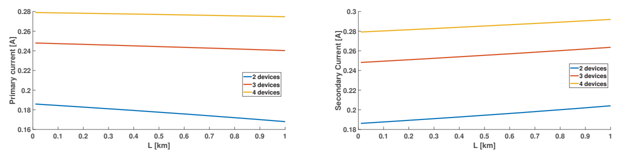

Fig. 8. Effect of the number of connected devices. RLC Model: primary (left) and secondary (right) emissions of harmonics $n°102$. $V_h = 94.61\angle - 4.56°V, R_g = 0.6153\Omega$

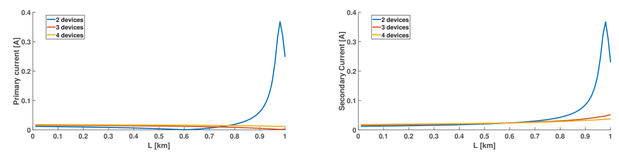

Fig. 9. Effect of the number of connected devices. RLC Model: primary (left) and secondary (right) emissions of harmonics $n°302$. $V_h = 54.37\angle - 4.56°V, R_g = 1.0587\Omega$

We are now able to draw some conclusions:

Primary emissions: the number of devices, as the length of the line, has not a big impact on the primary emissions when many devices are placed at the same point on the line. The grid resistance has an impact on the damping of the primary emission: when the resistance increases, the damping becomes more important.

Secondary emissions: when the grid resistance increases, the secondary emission increases as well because less current from the others devices will flow into the grid and will instead flow into device 1. The secondary emissions obviously increases with the number of devices.

Accuracy of the model: by considering only a simple R-modeled grid there is a significant loss of information. The introduction of the capacitance in the model has an effect in terms of resonances. This effect starts to appear at higher frequencies. It attenuates for the primary emission and amplifies for the secondary emission (see the values for $L = 500m$ in Fig.9).

B. Interaction between Two Devices at Different Points

The study of the propagation between more devices can be more relevant in a realistic situation, in which they are not connected at the same point in the grid. The experience consists in studying the interaction between two devices. The first is fixed to a position corresponding to 0 m of the line. In Fig.10, the position of the second device is varied until 250 m where it will be fixed. Fig. from 11 to 13 show a change in the point at which the device is fixed, respectively at 500 m, 750 m, 1 km. Only harmonics at 5100 Hz, 10050 Hz, 15100 Hz and 20050 Hz are presented.

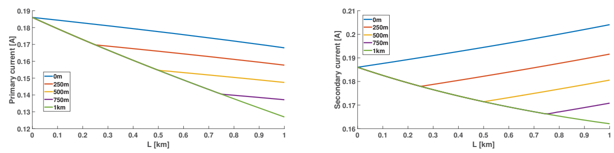

Fig. 10. Interaction between devices. Two devices at 250 m: primary (left) and secondary (right) emissions of harmonics $n°102$. $V_h = 94.61\angle - 4.56°V, R_g = 0.6153\Omega$

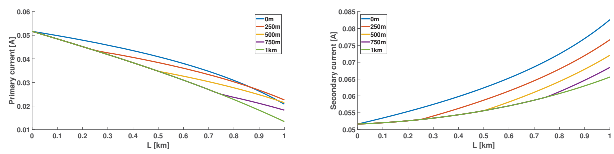

Fig. 11. Interaction between devices. Two devices at 500 m: primary (left) and secondary (right) emissions of harmonics $n°201$. $V_h = 103.38\angle - 2.28°V, R_g = 0.8637\Omega$

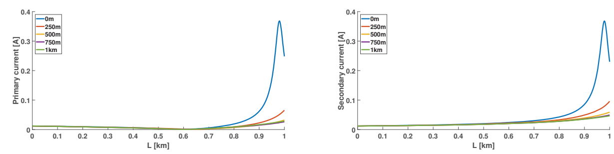

Fig. 12. Interaction between devices. Two devices at 750 m: primary (left) and secondary (right) emissions of harmonics $n°302$. $V_h = 54.37\angle - 4.56°V, R_g = 1.0587\Omega$

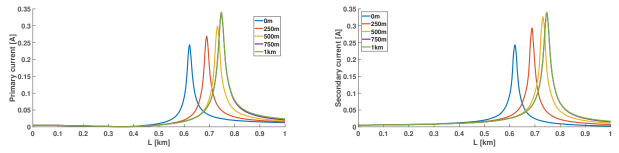

Fig. 13. Interaction between devices. Two devices at 1 km: primary (left) and secondary (right) emissions of harmonics $n°401$. $V_h = 41.04\angle - 2.28° V, R_g = 1.2199\Omega$

At low frequencies (see Fig.10 and Fig.11), the emissions are maximum when both devices are placed at the same point (blue line). At higher frequencies, resonances start to occur, so that the point at which the maximum emissions appear change accordingly to the harmonic (see Fig.12 and Fig.13). A maximum value of emissions is found in Fig. 12 for harmonic at 15100 Hz, where we obtain a value of 0.3682 A for the primary emission and 0.3677 A for the secondary emissions, both corresponding to the case of two devices at 980 m, in which a resonance occurs.

VI. Conclusions

The initial objective of this work was to implement a complete model running in a time-domain simulation to give the best accuracy. Unfortunately, this model proved to be far too slow to be practical, requiring several minutes of computation time to simulate, for instance, two devices in parallel for 1 second. Therefore, two main simplifications were proposed:

- The first simplification consisted in replacing the DC/DC converter of the complete model with a current source,
- The second simplification consisted in replacing the inverter with three voltage sources controlled by a MATLAB code generating the same harmonics.

Because of the range of frequencies we are interested in, we had to design a network model that was especially suitable for high frequencies.

Simulations showed that for many devices placed at the same point of the line, the number of the devices, as the length of the line, have not a big impact on the primary emission, whereas the grid resistance has an impact on the damping of the primary emission. On the contrary, the secondary emission grows as the resistance and the number of devices increase.

Another interesting result is that both primary and secondary emission are highly affected by increasing the complexity of the model of the grid: when moving at higher frequencies, the resonance can affect those values. In some cases, the resonance can also result in an attenuation for the primary emission and in an amplification for the secondary emission. We found the maximum emissions for the harmonics at 15100 Hz where we obtain a value of 0.3682 A for the primary emission and 0.3677 A for the secondary emissions, both corresponding to the case of two devices at a length of the line corresponding to 980 m, in which a resonance occurs.

In the end, we can conclude that there still remains a lack of knowledge that prevents us from understanding the origin and the spread of supraharmonics. Such knowledge is required to avoid future interference, but also to avoid the setting of unnecessary strict requirements on end-user equipment or on network operators. Models for equipment in this frequency range have to be further developed, in order to study the propagation of signals. The previous studies indicate that supraharmonics do not propagate beyond nearby devices. It has however been also shown that resonances are likely to occur. In this work, we brought to light a number of results that were obtained by simulation. Differential mode disturbances have to be investigated as well as interactions between different equipments. It would be useful to check them by laboratory experiments on a micro-network.

References

[1] Martin Lundmark: Design of low-voltage installations considering the spread of High-frequency harmonics. PhD thesis, Lulea University of Technology, Lulea, 2010.

[2] Ronnberg, S, Wahlberg, Mats ; Bollen, Math ; Lundmark, Martin; Equipment currents in the frequency range 9-95 kHz, measured in a realistic environment; International conference on harmonics and quality of power (ICHQP), September 2008.

[3] CENELEC, 2010, "SC205A Main communicating systems TF EMI Study report on electromagnetic interference between electrical equipment / systems in the frequency range below 150 kHz".

[4] CENELEC, 2013, "SC205A Main communicating systems TF EMI Study report on electromagnetic interference between electrical equipment / systems in the frequency range below 150 kHz (2nd edition)".

[5] CENELEC, 2015, "SC205A Main communicating systems TF EMI Study report on electromagnetic interference between electrical equipment / systems in the frequency range below 150 kHz (3rd edition)".

[6] G. Chicco, A. Russo, F. Spertino, "Supraharmonics: Concepts and Experimental Results on Photovoltaic Systems", 2015 International School on Nonsinusoidal Currents and Compensation (ISNCC)

[7] Matthias Klatt ; Jan Meyer ; Peter Schegner ; Christian Lakenbrink, "Characterization of Supraharmonic Emission Caused by Small Photovoltaic Inverters", Mediterranean Conference on Power Generation, Transmission, Distribution and Energy Conversion (MedPower 2016)

[8] M. Ahmadi, N. M. and R. Sharma. "A Review on Topologies for Fast Charging Stations for Electric Vehicles". University of Queensland Brisbane, Australia. 2016.

[9] F. Adinolfi, F. Conte, S. Massucco, M. Saviozzi, F. Silvestro, S. Grillo, "Performance evaluation of algorithms for the State of Charge estimation of storage devices in microgrid operation ", in 19th Power Systems Computation Conference, June 2016

[10] A. Aranciba, K. Strunz. "Modeling of an Electric Vehicle Charging Station for Fast DC Charging". Proceedings of the 2012 IEEE International Electric Vehicle Conference (IEVC).

[11] Min-Young Park, Min-Hun Chi, Jong-Hyoung Park, Heung-Geun Kim, Tae-Won Chun, Em-Cheol Nho, "LCL-filter design for grid-connected PCS using total harmonic distortion and ripple attenuation factor". Power Electronics Conference (IPEC), 2010 International , vol., no., pp.1688-1694, 21-24 June 2010.

[12] MathWorks. (2014). ode23tb. https://it.mathworks.com/help/physmod/sps/powersys/ref/battery.html

[13] BLACK, H.S.: "Modulation theory" (Van Nostrand, 1953).

[14] The MathWorks. (2013). Three-Phase PI Section Line. https://it.mathworks.com/help/physmod/sps/powersys/ref /threephasepisectionline.html

[15] Uytterhoeven, S. (2008). Determination of LV-cable parameters through measurement and fitting on the cable model. Linkebeek: Laborelec.

[16] Nexans. (s.d.). Cbles de rseau basse tension et cbles moyenne tension.

[17] Benchmark Systems for Network Integration of Renewable and Distributed Energy Resources.15 May 2013. Task Force C6.04.02.

[18] Transmission Line Reference Book 345 kV and Above, 2nd ed., Electric Power Research Institute, Palo Alto, California, 1987. With permission. Glover, J.D. and Sarma, M.S., Power System Analysis and Design, 3rd ed., Brooks=Cole, 2002. With permission.